arXiv:1207.5109v1 [astro-ph.CO] 21 Jul 2012

Observational Manifestations of the First Protogalaxies in the 21 cm Line*

E. O. Vasiliev[1,2]†, Yu. A. Shchekinov[2,3]
[1]*Institute of Physics, Southern Federal University, Rostov-on-Don, Russia*
[2]*Physics Department, Southern Federal University, Rostov-on-Don, Russia*
[3]*Special Astrophysical Observatory, Russian Academy of Sciences,*
Nizhnyi Arkhyz, Karachay-Cherkessia Republic, Russia

Abstract

The absorption properties of the first low-mass protogalaxies (mini-halos) forming at high redshifts in the 21-cm line of atomic hydrogen are considered. The absorption properties of these protogalaxies are shown to depend strongly on both their mass and evolutionary status. The optical depths in the line reach ∼0.1-0.2 for small impact parameters of the line of sight. When a protogalaxy being compressed, the influence of gas accretion can be seen manifested in a non-monotonic frequency dependence of the optical depth. The absorption characteristics in the 21-cm line are determined by the thermal and dynamical evolution of the gas in protogalaxies. Since the theoretical line width in the observer's reference frame is 1-6 kHz and the expected separation between lines 8.4 kHz, the lines from low mass protogalaxies can be resolved using ongoing and future low frequency interferometers.

1 Introduction

One of the means of studying the history of intergalactic space before the epoch of secondary ionization (reionization) of hydrogen is radio observations in the 21-cm line of neutral hydrogen [1-3]. At least three methods for studying this epoch have been proposed: (1) observations in emission or absorption in the neutral intergalactic medium against the global cosmic microwave background (CMB) signal [4, 5], (2) statistical studies of the angular distribution of the signal fluctuations [6, 7], and (3) observations of absorption in the spectrum of a distant strong radio source, which may reveal a "forest" in the 21- cm line (analogous to the Lα forest in the optical spectra of quasars and galaxies) [8-10]. The first two methods involve mapping spatial (position on the sky) and temporal (redshift) properties of the intergalactic medium, while the latter provides information only along a line of sight as a function of redshift. Since the spatial scales corresponding to the angular resolutions of ongoing or futture radio telescopes, such as LOFAR[1] are roughly 1 Mpc, only large-scale structures, such as giant ionization regions around massive galaxies and quasars, can be observed. Measurements of absorption at different redshifts can be used to resolve small-scale structures, individual protogalaxies (mini-halos), and ionization zones in low-mass protogalaxies.

The effect of external ionizing radiation on the properties of the 21-cm forest was studied in [9-14]. Mainly, the dark-matter profiles in protogalaxies have been taken to be steep (cusped) [15]. However, observations of dwarf galaxies in the local Universe indicate a "flat" distribution of dark matter (a truncated isothermal sphere with a flat core) [16]. Recent theoretical studies have

*Astronomy Reports, 2012, Vol. 56, No. 2, pp. 77-83.
†eugstar@mail.ru
[1]http://www.lofar.org/index.htm

also found that the first protogalaxies could have flat dark-matter profiles [17-19]. The first halos were assumed in [9, 10] to be virialized and isothermal, and their absorption characteristics were calculated without accounting of the gas and dark matter evolution. Some evolutionary effects were included in [14], such as a possible influence of gas accretion and star formation, although the gas and dark matter profiles of minihalos before the first stars have appeared were assumed to be time-independent. It is well known though that the density inside the perturbation from which a protogalaxy does form increases by more than a factor of 200 in the non-linear stage, facilitating cooling of the gas and a decrease of its ionization fraction [20-23]. It is obvious that such appreciable evolutionary variations in the physical properties of the gas could substantially affect absorption properties of the first protogalaxies. With this in mind, Meiksin [13] considered possible variations in the absorption properties caused by the virialization process of the first protogalaxies.

Here, we investigate the absorption properties of the first protogalaxies within a self-consistent, one-dimensional, spherically symmetric description of their thermal and chemical evolution. In the heirarchical scenario of galaxy formation, the first protogalaxies able collapse and lead to formation of the first stars had low masses. The minimum mass of the first protogalaxies, $M_h \sim 10^7\ M_\odot$ at redshifts $z \sim 10$, was apparently determined by molecular-hydrogen cooling [23]. We will study the 21-cm profiles for mini-halos with masses near this minimum mass, with the aim of using possible differences in the 21-cm absorption characteristics as a tool to answer the question of whether the minimum masses of halos in which star formation began were indeed close to $M_h \sim 10^7\ M_\odot$ at $z \sim 10$. Section 2 describes the model used, Sections 3 and 4 present our results and conclusions. The computations assume a ΛCDM cosmological model with $(\Omega_0, \Omega_\Lambda, \Omega_m, \Omega_b, h) = (1.0,\ 0.76,\ 0.24,\ 0.041,\ 0.73)$, and a relative number density of deuterium of $n[\mathrm{D}]/n = 2.78 \cdot 10^{-5}$ [16].

2 Evolution of minihalos

We modeled evolution of the first protogalaxies using a one-dimensional Lagrangian approach similar to that proposed in [23]. It is difficult to fully take into account mergers of protogalaxies and other essentially non-one-dimensional dynamical effects in such a simple model. This would require self-consistent, three-dimensional cosmological simulations with high resolution, which is not currently possible. By necessity therefore we will use simplified model approximations that are commonly applied to reduce multi-dimensional problems to spherically symmetric ones.

2.1 Dynamics of Dark Matter

The description of dark matter in our model is analogous to that of [23]. It is assumed that dark matter with the mass $M_{DM} = \Omega_{DM} M_{halo}/\Omega_m$ is contained inside the radius R_{tr} and has a truncated isothermal sphere profile with a flat core of radius R_{core}, here Ω_m is the matter density and $\Omega_{DM} = \Omega_m - \Omega_b$. The ratio $\xi = R_{core}/R_{vir}$ is assumed through the paper to be 0.1; R_{vir} is the virial radius of the halo, outside the radius R_{tr} , the dark-matter density is equal to the background cosmological value, $\rho_{DM} = \rho_0 \Omega_{DM} (1+z)^3$, where $\rho_0 = 1.88 \times 10^{-29} h^2$ is the critical density; the radii R_{tr} and R_{core} evolve in time [23]. Such a description is usually accepted to imitate the evolution of density perturbations (see, e.g., [25]). Before the "turnaround" point, i.e. the point where the perturbation separates from the Hubble flow, the density within the truncated sphere, $R < R_{tr}$, varies with time similarly to what approximated in [21]

$$\rho = \rho_0 \Omega_{dm} (1+z)^3 \exp\left(\frac{2.8A}{1 - 0.5A^2}\right), \qquad (1)$$

where $A = (1 + z_{vir})/(1 + z)$. We accept in (1) the numerical coefficients in the exponent slightly different from the ones used in [21], in order to achive a better agreement between (1) and the

exact solution in the vicinity of the turnaround point. The approximation (1) violates near the virialization point, however this is not important for our purposes, since it is not used beyond the turnaround point.

2.2 Gas Dynamics and Chemical Kinetics

For modeling evolution of the gas (i.e., the baryonic component of a protogalaxy) a one-dimensional spherically symmetric Lagrangian scheme similar to that described in [26] is used. The standard resolution in the computations is 1000 cells (spherical shells), which provides a sufficiently good convergence of the scheme.

Chemical kinetics of the primordial gas includes the following main components H, H^+, e, H^-, He, He^+, He^{++}, H_2, H_2^+, D, D^+, D^-, HD, HD^+. The corresponding reaction rates are taken from [27, 28]. In the energy equation radiative losses typical for the primordial gas: cooling with recombination, collisional excitation of hydrogen and helium, free-free transitions, Compton interactions with CMB photons [29], and molecular cooling via H_2 [28] and HD [30, 31] are accounted.

All models begin at the redshift $z = 100$, when the density perturbations are small and obviously linear. The initial parameters for $z = 100$, i.e., the gas temperature, ion and molecular composition, etc, are found from a one-zone calculateion starting at $z = 1000$ with the standard gas parameters for the end of the recombination epoch: $T_{gas} = T_{CMB}$, $x[\mathrm{H}] = 0.9328, x[\mathrm{H}^+] = 0.0672, x[\mathrm{D}] = 2.3 \times 10^{-5}, x[\mathrm{D}^+] = 1.68 \times 10^{-6}$ (see [23, Table 2] for details and references). The initial size of the computational domain is 10 virial radii for a protogalaxy of a given mass.

2.3 The 21 cm Line

Only collisional excitation by atoms and electrons is taken into account when computing the spin temperature for the 21-cm line [32]:

$$T_s = \frac{T_{CMB} + y_c T_k}{1 + y_c} \tag{2}$$

where T_{CMB} is the temperature of the CMB, y_c is a function determined by the efficiency of collisional excitation

$$y_c = \frac{C_{10} T_*}{A_{10} T_k}, \tag{3}$$

$T_* = 0.0682$ K is the energy for the transition between sublevels of the hyperfine structure, $A_{10} = 2.87 \times 10^{-15}$ s^{-1} is the transition probability, $C_{10} = k_{10} n_H + \gamma_e n_e$ is the rate of collisional de-excitation by hydrogen atoms and electrons (we neglect the contribution from protons), the approximations for k_{10} of [33] and for γ_e from [34] are used. The computations do not take into account the influence of resonance ultraviolet radiation (UV pumping) on the level populations [35], since at redshifts $z = 10 - 15$ this effect can be important only locally near galaxies with star formation. At lower redshidt the regions of penetration of UV radiation from the stellar population become substantially greater and overlap and manifest reionization of the Universe. Moreover, in order for the contribution from UV pumping to the variations of the spin temperature to be comparable to the contribution from collisions, the flux of resonance UV radiation must be fairly high: $F_{Ly\alpha} \gtrsim 0.1$ erg s^{-1} cm^{-2} (this estimate is for typical temperatures $T \sim 200$ K and gas densities $n \sim 1$ cm^{-3} in protogalaxies at $z \sim 10$).

3 Absorption in the 21 cm line

We will study two observable quantities that describe the absorption properties of the gas in protogalaxies: the optical depth at frequency ν along the line of sight, and the total absorption

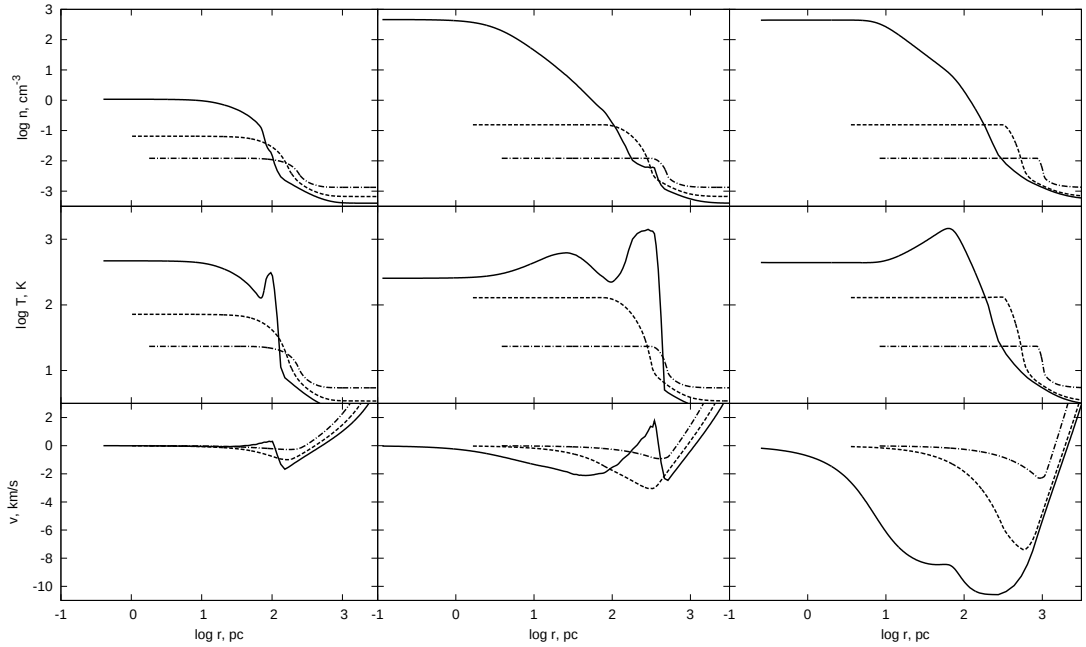


Figure 1: Number density, temperature, and velocity (from top to bottom) of the gas in protogalaxies with masses of 10^5, 10^6 and $10^7 M_\odot$ (from left to right) at times $z_{ta} = 15.5$ (dot-dashed curve), $z = 12$ (dashed curve), and $z_v = 10$ (solid curve).

within the protogalaxy, i.e., the line equivalent width. We consider the properties of low-mass protogalaxies (mini-halos) with masses of 10^5, 10^6 and $10^7 M_\odot$, which separated from the Hubble flow at redshift $z_{ta} \simeq 15.5$ and virialized by $z_v \simeq 10$.

Evolution of the first protogalaxies depends critically on their masses: low-mass protogalaxies cannot cool rapidly and form stars after their virialization. With increasing protogalaxy mass the number density of hydrogen molecules in the central regions grows, facilitating cooling of the gas and formation of the first stars (see [20-23, 36] for more detail). Figure 1 presents radial profiles of the gas density, temperature, and velocity in protogalaxies with masses of 10^5, 10^6 and $10^7 M_\odot$ at times close to the turnaround ($z_{ta} = 15.5$) and the virialization ($z_v = 10$), and also at a time corresponding to the intermediate redshift ($z = 12$). When virialized at $z_v = 10$, only protogalaxies with masses $M \gtrsim 10^7 M_\odot$ can form stars [22, 23]. In the process of virialization, gas density in the central regions already reaches $n \gtrsim 10^{8\ -3}$ at $z \simeq 11$, which essentially corresponds to the collapse and the onset of formation of the first pre-stellar cores. Therefore, for the virial state of the mass $M = 10^7 M_\odot$ we present the absorption characteristics corresponding to $z \simeq 11$, while for the two other masses the characteristics are calculated for $z_v = 10$. As noted above, in lower-mass protogalaxies, the prestellar cores either form after virialization or do not form at all.

The optical depth at frequency ν along a line of sight passing a distance α from the center of

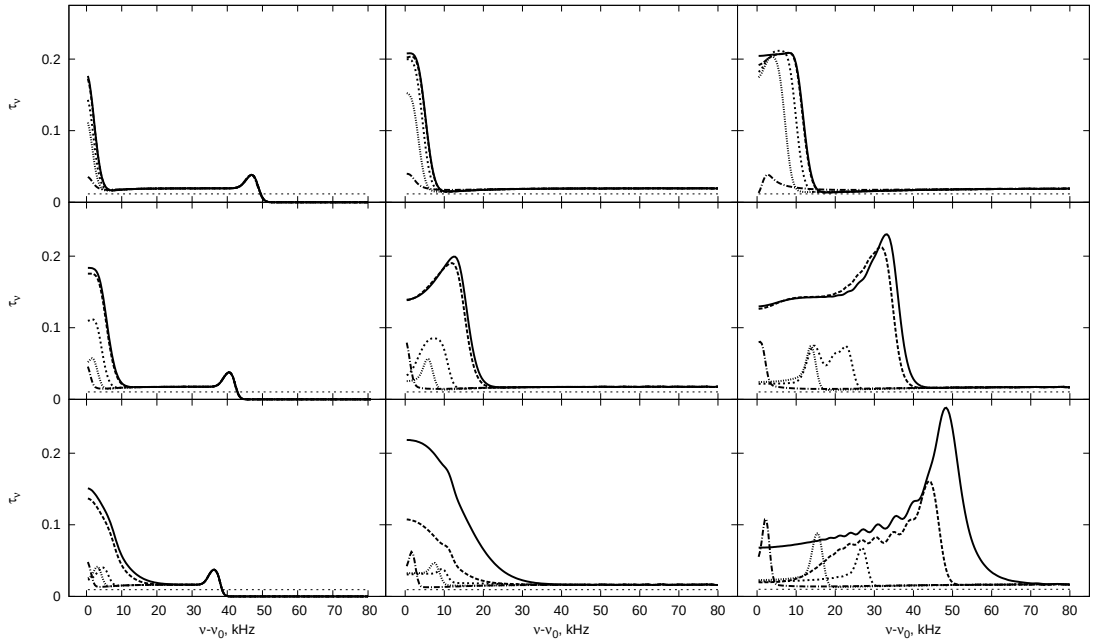


Figure 2: Optical depth for protogalaxies with masses of 10^5, 10^6 and $10^7 M_\odot$ (from left to right) at times $z_{ta} = 15.5$ (upper panel), $z = 12$ (middle panel), and $z_v = 10$ (lower panel). The curves correspond to the line of sight impact parameters $\alpha = 0.1, 0.3, 1, 1.5, 3r_{vir}$ (from right to left), and the thin dashed line to the background optical depth.

the protogalaxy is

$$\tau_\nu = \frac{3h_p c^3 A_{10}}{32\pi k \nu_0^2} \int_{-\infty}^{\infty} dR \frac{n_{HI}(r)}{\sqrt{\pi} b^2(r) T_s(r)} \exp\left[-\frac{[v(\nu) - v_l(\alpha, R)]^2}{b^2(r)}\right] \tag{4}$$

where $r^2 = \alpha^2 + R^2$, $v(\nu) = c(\nu - \nu_0)/\nu_0$, $v_l(\alpha, R)$ is the gas infall velocity projected on to the line of sight, $b^2 = 2kT_k(r)/m_p$ is the Doppler parameter, and the remaining notations are standard.

Figure 2 shows the optical depths for lines of sight passing at several impact parameters for protogalaxies with masses of 10^5, 10^6 and $10^7 M_\odot$ at times close to the turnaround ($z_{ta} = 15.5$) and the virialization time ($z_v = 10$), as well as at a time corresponding to the intermediate redshift $z = 12$. Considerable differences in the line absorptions are clearly visible, both for protogalaxies with different masses and during the evolution of a protogalaxy of a given mass. At $z = 15.5$ (upper panel in Fig. 2), the gas densities and temperatures in the protogalaxies with different masses are nearly the same (Fig. 1), and the differences in the line profiles are determined by the distributions of the gas velocity: with increasing protogalaxy mass the accretion velocity increases from $\sim$0.2 km/s for $10^5 M_\odot$ to $\sim$2 km/s for $10^7 M_\odot$. The small peak in the optical depth near $\nu - \nu_0 \simeq 40$ kHz and the drop to zero at higher frequencies for $M = 10^5 M_\odot$ is, from one side, due to the drop in the temperature at the periphery of the protogalaxy and the transition to the background value [a decrease in the denominator in the exponent (4)], and from the other due to the transition of

the velocity profile to the Hubble expansion [an increase in the numerator in the exponent (4)]. In more massive protogalaxies, a similar peak in optical depth is located at higher frequencies.

The absorption characteristics change considerably as the protogalaxy is compressed. At redshift $z = 12$ (middle panel in Fig. 2), the absorption lines become broader, and features due to the gas dynamics during the collapse of the protogalaxies appear. In low-mass protogalaxies ($M = 10^5 M_\odot$), the enhancement of gas velocity in the accretion shock is modest, so that the absorption line profiles for the various impact parameters of the line of sight broaden only slightly. In higher-mass protogalaxies ($M \gtrsim 10^6 M_\odot$), the accretion wave is stronger, and a stronger jump in the temperature and density arises, which manifests a nonmonotonic frequency dependence of the optical depth for the lines of sight intersecting this region ($\alpha \lesssim r_{vir}$) as, more precisely, a decrease in the optical depth in the line center.

At $z = 10$ (at $z \simeq 11$ for $M = 10^7 M_\odot$), the absorption-line profiles depend substantially on differences in the dynamical and thermal evolution of the protogalaxies (lower panels in Figs. 1 and 2): the lines become appreciably broader, the strongest absorption is observed for $\alpha \lesssim 0.3 r_{vir}$, the influence of gas accretion is clearly seen in the protogalaxy with mass $M = 10^7 M_\odot$ resulting in pronounced peaks in the frequency dependence of the optical depth. In more massive protogalaxies gas cools more efficiently, and, moreover, the shocks associated with virialization appear to be stronger in more massive protogalaxies. Note that the line profile for $M = 10^6 M_\odot$ at $z = 10$ has changed since $z = 12$: contrary to $z = 12$ at $z = 10$ the optical depth falls off essentially monotonically from the line center. This is due to a decrease in the accretion, and the appearance of a reverse shock acting to oppose the accretion (Fig. 1). In the case of higher-mass protogalaxies ($M = 10^7 M_\odot$), the accretion increases with decreasing redshift, while the non-monotonic dependence of the optical depth becomes stronger.

Let us now investigate how thermal evolution affects the absorption-line profiles. For this purpose, we calculate the evolution of a protogalaxy with mass $M = 10^6 M_\odot$ without radiation gas cooling in atomic and molecular processes (i.e. we consuder the adiabatic case), and compare it with the results described above (Fig. 3). In the presence of radiation cooling the central regions of the protogalaxy are seen to cool efficiently during virialization, and the radial dependences differ considerably from the adiabatic case, but these differences are substantial only in the inner region of the protogalaxy, $\alpha \lesssim 0.5 r_{vir}$, where the effects of cooling are stronger due to the higher density. As a result, the absorption line profiles will also differ in this region as seen in Fig. 4.

Another observational characteristic is the line equivalent width, $\langle \Delta\nu \rangle_{obs} = \langle \Delta\nu \rangle_i / (1+z)$, where the rest-frame equivalent width is

$$\frac{\langle \Delta\nu_i \rangle}{2} = \int_{-\infty}^{\infty} (1 - e^{-\tau_\nu}) d\nu - \int_{-\infty}^{\infty} (1 - e^{-\tau_{IGM}}) d\nu \tag{5}$$

where τ_{IGM} is the background optical depth of the neutral intergalactic medium. Figure 5 presents the observed line equivalent width for absorption in protogalaxies with masses of 10^5, 10^6 and $10^7 M_\odot$ at redshifts $z = 15.5, 12$, and 10. The equivalent width depends only weakly on the impact parameter of the line of sight at $z = 15.5$, but in the process of formation of a protogalaxy it grows at $\alpha \lesssim r_{vir}$, reaching 0.1-0.4 kHz for $M = 10^6 - 10^7 M_\odot$. The line width of the perturbations after separation from the Hubble flow in the observer's rest frame (i.e. at $z = 0$) equals to 1-6 kHz. Since the distance between the lines is $\sim$8 kHz at $z = 10$ [14], and the spectral resolution of 0.76 kHz can be reached with existing and planned low-frequency interferometers, such as LOFAR and the SKA[2] the lines of low-mass protogalaxies might be quite resolvable with these instruments.

Note that when describing the initial growth of a density perturbation after recombination, it is assumed that the velocities of the dark matter and baryons are similar and their relative velocities low [37]. This picture has been recently supplemented with a possibility of supersonic relative motions of baryons and dark matter with velocities $v_s(z) = v_{s,i}/(1+z)$, where $v_{s,i}$ is the

[2]http://www.skatelescope.org/

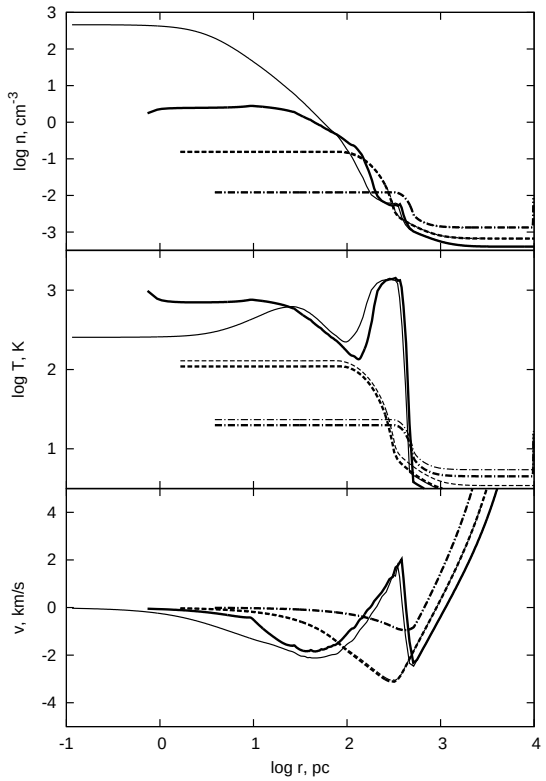


Figure 3: Density, temperature, and velocity (from top to bottom) in a protogalaxy with mass $10^6 M_\odot$ at times $z_{ta} = 15.5$ (dot-dashed curve), $z = 12$ (dashed curve), and $z_v = 10$ (solid curve), with (thin curves) and without (thick curves) taking into account cooling of the gas. The difference is clearly seen at the virialization time $z_v = 10$; these curves coincide at the other two times considered.

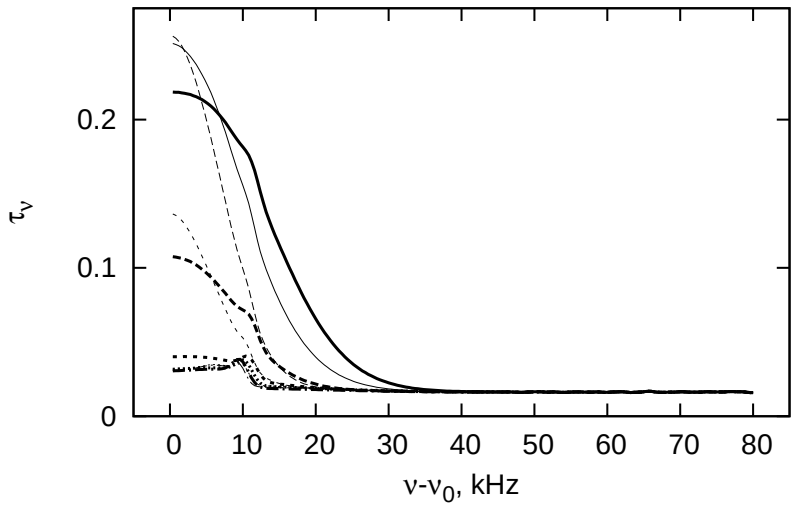


Figure 4: Optical depth for a protogalaxy with mass $10^6 M_\odot$ at time $z_v = 10$. The curves correspond to the line of sight impact parameters $\alpha = 0.1, 0.3, 0.5, 0.8, 1 r_{vir}$ (from right to left) with (thin curves) and without (thick curves) radiation gas cooling. The difference is clearly seen for $\alpha \lesssim 0.5 r_{vir}$; the curves coincide for higher values of α.

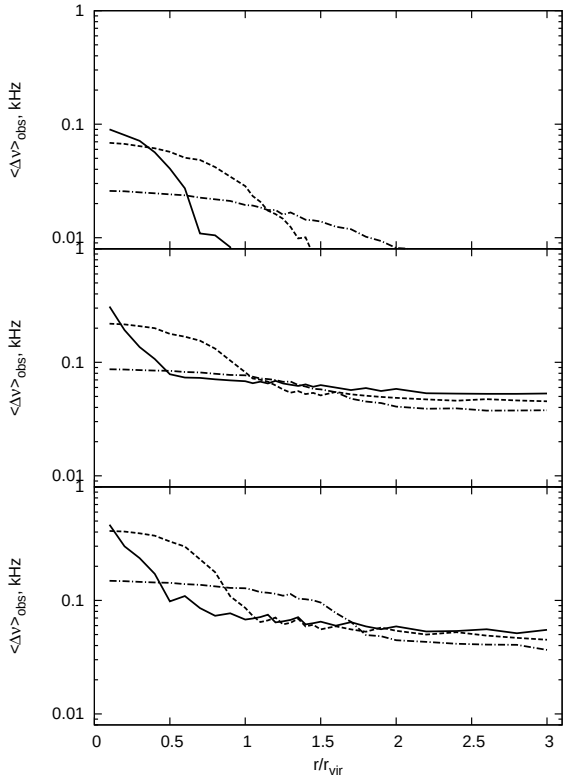


Figure 5: Observed line equivalent width for protogalaxies with masses of 10^5, 10^6 and $10^7 M_\odot$ (from top to bottom) at times $z_{ta} = 15.5$ (dot-dashed curve), $z = 12$ (dashed curve), and $z_v = 10$ (solid curve).

rms relative velocity of the gas at the epoch of recombination [38]. It is assumed that, during the compression of protogalaxies, their gas moves with an effective speed $v_{eff} = \sqrt{c_s^2 + v_s^2}$ (c_s is the sound speed) [39]. We carried out computations of the evolution of protogalaxies with masses of $M = 10^5 - 10^7\ M_\odot$ taking into account $v_s(z)$, adopting the characteristic value $v_{s,i} = 30$ km/s for the epoch of recombination [38]. It was found that compared to the standard case described above (Fig. 2) the accounting of the relative motion of baryons and dark matter results in an approximately 10-30% decrease in the optical depth in the 21-cm line at the epoch of separation of the perturbation from the Hubble flow. For more massive protogalaxies this change is smaller and decreases by the epoch of virialization, while for low-mass protogalaxies remains considerable comprising about 10%.

4 Conclusions

We have used one-dimensional, spherically symmetric computations to investigate the absorption properties of the first protogalaxies in the 21-cm line of HI at the lower mass boundary admitting the collapse of baryons and star formation, $M_h \leq 10^7\ M_\odot$ at $z \gtrsim 10$. We have studied the evolution of the 21-cm line profile and observed equivalent width during the virialization of these protogalaxies.

The absorption properties of the protogalaxies depend substantially on both their mass and their evolutionary status. The optical depth in the line reaches $\sim 0.1 - 0.2$ at small line of sight impact parameters for protogalaxies with masses of $M = 10^5 - 10^6 M_\odot$, then monotonically falls off to the background value. The 21-cm absorption profiles for halos with masses of $M = 10^7\ M_\odot$ and probably higher masses differ qualitatively from the profiles of the halos with masses below this lower limit: massive halos show a dip at the line center. This can be used to observationally determine the minimum masses of protogalaxies; i.e., of minihalos capable to cool radiatively, and enabling the collapse of baryons with subsequent star formation.

The influence of gas accretion, manifested as a nonmonotonic frequency dependence of the optical depth, can be seen as the protogalaxies are compressed. The accretion wave is observed at large line-of-sight impact parameters for protogalaxies with masses $M \simeq 10^5 M_\odot$, and becomes stronger for protogalaxies with higher masses ($M \gtrsim 10^6 M_\odot$), leading to a large jump in the gas temperature and density, which gives rise to appreciable peaks in the frequency dependence of the optical depth for $\alpha \lesssim r_{vir}$. The absorption properties are mostly determined by the thermal and dynamical evolution of the gas in the protogalaxies.

The equivalent width corresponding to the turnaround point in the observers rest frame (i.e., $z = 0$) depends only weakly on the line-of-sight impact parameter α, but grows with the formation (virialization) of protogalaxies with masses of $M = 10^6 - 10^7 M_\odot$, reaching 0.1-0.4 kHz for $\alpha \lesssim 0.5 r_{vir}$. The expected distance between lines is 8.4 kHz at $z \sim 10$ [14], that is larger than the width of the 21 cm absorption lines from low mass protogalaxies in the observers rest frame, so that the lines can be resolved using low frequency ongoing and future interferometers.

5 Acknowledgements

This work was supported by the Russian Foundation for Basic Research (project codes 09-02-00933, 11-02-90701) and the Ministry of Education and Science of the Russian Federation, in the framework of the Federal Targeted Program The Scientific and Science Education Staff of Innovative Russia for 2009-2013 (state contracts 02.740.11.0247 and P-685) and the Analytical Departmental Targeted Program The Development of the Scientific Potential of Higher Education RNP-2.1.1/11879.

References

[1] C.J. Hogan, M.J. Rees, Mon. Not. Roy. Astron. Soc. **188**, 791 (1979)

[2] D. Scott, M.J. Rees, D. Sciama, Astron. and Astropys. **250**, 295 (1991)

[3] P. Madau, A. Meiskin, M.J. Rees, Astrophys. J. **475**, 492 (1997)

[4] P.A. Shaver, R.A. Windhorst, P. Madau, A.G. de Bruyn, Astron. and Astropys. **345**, 380 (1999)

[5] S.K. Sethi, Mon. Not. Roy. Astron. Soc. **363**, 818 (2005)

[6] P. Tozzi, P. Madau, A. Meiskin, M.J. Rees, Astrophys. J. **528**, 597 (2000)

[7] I.T. Iliev, P.R. Shapiro, A. Ferrara, H. Martel, Astrophys. J. Lett. **572**, 123 (2002)

[8] C.L. Carilli, N.Y. Gnedin, F. Owen, Astrophys. J. **577**, 22 (2002)

[9] A. Kumar, T. Padmanabhan, K. Subramanian, K., Mon. Not. Roy. Astron. Soc. **272**, 544 (1995)

[10] J.S. Bagla, B.B. Nath, T. Padmanabhan, Mon. Not. Roy. Astron. Soc. **289**, 571 (1997)

[11] S.R. Furlanetto, A. Loeb, Astrophys. J. **579**, 1 (2002)

[12] S.R. Furlanetto, Mon. Not. Roy. Astron. Soc. **370**, 1867 (2006)

[13] A. Meiksin, Mon. Not. Roy. Astron. Soc., , arXiv:1102.1362

[14] Y. Xu, A. Ferrara, X. Chen, Mon. Not. Roy. Astron. Soc. **410**, 2025 (2011)

[15] J.F. Navarro, C.S. Frenk and S.D.M. White, Astrophys. J. **490**, 493 (1997)

[16] A. Burkert, Astrophys. J. Lett. **447**, 25 (1995)

[17] S. Mashchenko, H.M.P. Couchman, J. Wadsley, Nature **442**, 539 (2006)

[18] C. Tonini, A. Lapi, P. Salucci, Astrophys. J. **649**, 591 (2006)

[19] E.V. Mikheeva, A.G. Doroshkevich, V.N. Lukash, Nuovo Cim. B **122**, 1393 (2007)

[20] Z. Haiman, A. Thoul, A. Loeb, Astrophys. J. **464**,523 (1996)

[21] M. Tegmark, J. Silk, M.J. Rees, A. Blanchard, T. Abel, F. Palla, Astrophys. J. **474**, 1 (1997)

[22] E.O. Vasiliev, Yu.A. Shchekinov, Astron. Rep. **47**, 979 (2003)

[23] E. Ripamonti, Mon. Not. Roy. Astron. Soc. **376**, 709 (2007)

[24] D.N. Spergel, R. Bean, O. Doré, et. al., Astrophys. J. Suppl. Ser. **170**, 377 (2007)

[25] T. Padmanabhan, Structure Formation in the Universe, Cambridge Univ. Press, Cambridge (1993)

[26] P.C. Stancil, S. Lepp, A. Dalgarno, A., Astrophys. J. **509**, 1 (1998)

[27] A. Thoul, D. Weinberg, Astrophys. J. **442**, 480 (1995)

[28] D. Galli, and F. Palla, Astron. and Astropys. **335**, 403 (1998)

[29] R. Cen, Astrophys. J. Suppl. Ser. **78**, 341 (1992)

[30] D. Flower, Mon. Not. Roy. Astron. Soc. **318**, 875 (2000)

[31] A. Lipovka, R. Núñez-López, V. Avila-Reese, Mon. Not. Roy. Astron. Soc. **361**, 850 (2005)

[32] G.B. Field, Proc. IRE **46**, 240 (1958)

[33] M. Kuhlen, P. Madau, R. Montgomeri R., Astrophys. J. Lett. **637**, 1 (2006)

[34] H. Liszt, Astron. and Astropys. **371**, 698 (2001)

[35] S. Wouthuysen, Astron. J., **57**, 31 (1952)

[36] B. Ciardi, A. Ferrara, Spa. Sci. Rev., **116**, 625 (2005)

[37] Y. B. Zeldovich, Astron. and Astropys. **5**, 84 (1970)

[38] D. Tseliakhovich, C. Hirata, Phys. Rev. D., **82**, 083520 (2010)

[39] A. Stacy, V. Bromm, A. Loeb, Astrophys. J. Lett., **730**, 1 (2011)